Stochastic resonance and spike-timing precision in an ensemble of leaky integrate and fire neuron models

T. Shimokawa,[1] A. Rogel,[2] K. Pakdaman,[1] and S. Sato[1]
[1]*Department of System and Human Science, Graduate School of Engineering Science, Osaka University, Toyonaka, 560-8531 Osaka, Japan*
[2]*Centre de Bioinformatique, INSERM U444, Université Paris 7 2 Place Jussieu, 75251 Paris Cedex 5, France*
(Received 30 September 1998)

We analyze the transmission of sinelike periodic signals by an ensemble of leaky integrate-and-fire neuron models in the presence of additive noise. We observe that when the number of units in the ensemble is large enough, the point process formed by pooling the spike trains of all units is an inhomogeneous Poisson process. We obtain the intensity of this process, i.e., the instantaneous discharge rate of the ensemble, from the cycle histogram of the discharge of a single unit. This enables us to link measures of the regularity of the output discharge rate and the transmission of the periodic input, such as the signal to noise ratio and the input-output power norm and normalized power norm directly to the shape of the cycle histogram. Furthermore, we also show that firing precision in response to subthreshold stimulation is maximized at some intermediate noise value, and argue that in this regime the ensemble can reliably transmit fast periodic signals below the resolution of the individual units. Our analysis clarifies the conditions whereby noise enhances signal transmission and detection in ensembles. [S1063-651X(99)09803-7]

PACS number(s): 87.10.+e, 07.05.Mh

I. INTRODUCTION

Sensory neurons transform signals from the environment into trains of spikes that propagate to other structures in the nervous system. Since internal and external noise are ubiquitous and unavoidable, many studies have investigated their effect on signal transmission by sensory neurons. These have shown that noise of appropriate amplitude linearizes the response of neurons, leads to stochastic resonance (SR), and maximizes input-output correlation (power norm), transinformation and coherence [1]. These phenomena have received considerable attention because of the surprisingly beneficial effect of noise, and theoretical analyses aim to clarify the conditions under which they occur [2,3]. For reviews on SR, see [4].

In this work, we evaluate the effect of pooling the response of a large number of neurons in parallel on the aforementioned phenomena as such architecture may be involved in sensory systems. The importance of the study of the influence of noise on signal transduction across ensembles was stressed in [5]. These authors showed that in the presence of appropriate noise, such ensembles can reliably detect subthreshold pulses, through synchronous firing. Prior to their study, the prevailing view was that noise would mainly deteriorate firing precision, so that noisy ensembles would encode incoming signals into rate codes obtained through averaging the response of all units [6]. This standpoint was further supported by the fact that the input-output transduction fidelity of large ensembles is relatively insensitive to noise intensity, when this quantity is large enough [7–9].

In this study, we examine the two situations, that is the influence of noise on both rate and temporal coding schemes, in the same system. In this way, we intend to characterize the noise intensities that would be adequate for one regime rather than the other. This should help, in principle, to better understand the conditions under which each scheme may be operating in nervous systems.

More precisely, we study the influence of additive noise on the response of an ensemble of leaky integrate and fire model (LIFM) units to periodic stimulation. The choice of the model was motivated by the fact that the LIFM captures the essential properties of neurons, that is excitability and postdischarge refractoriness, so that the results should hold for more complex models and living neurons. The input signal was selected as a periodic one because of its biological relevance. Well studied examples of precise temporal coding in nervous systems, such as in the electro-sensory system of the fish eigenmannia [10] and the auditory system of the barn owl [11] rely on firing at a given phase of a periodic modulation. Furthermore, the possible role of the interplay between subthreshold modulation and noise has also been observed in the shark temperature sensitive electroreceptors [12]. Finally, theoretical studies have indicated how nervous systems may learn and process information using this form of temporal coding [13,14].

This paper is organized as follows. In Sec. II, we describe the model of the ensemble of LIFMs. In Sec. III, we construct a statistical model of the discharge train of this system. This model is valid for subthreshold and suprathreshold, as well as slow or fast periodic stimulation. We use this statistical model to determine the noise levels that maximize input-output fidelity (Sec. IV A), and discharge timing precision (Sec. IV B). We compare the corresponding regimes in Sec. IV C. Finally we discuss our results in Sec. V.

II. THE ENSEMBLE MODEL

We consider an ensemble of N LIFM units receiving the same periodic stimulation and independent noise. Each

LIFM is characterized by its membrane potential, denoted by V_i. Whenever V_i overtakes a constant threshold S_0, a spike is generated, following which, V_i is reset to a post-discharge hyperpolarization V_0. Between successive discharges, V_i is determined by

$$dV_i = \left[-\frac{V_i - V_r}{\tau} + A\sin(\Omega t + \theta_0) \right] dt + D\,dW_i, \quad (2.1)$$

where V_r is the resting potential, τ is the characteristic charge-discharge time of the membrane, A, Ω, and θ_0 are, respectively, the amplitude, the angular velocity $2\pi/T$ and the initial phase of the stimulation, D is the noise amplitude and dW_i are independent white Gaussian noise. Thus, all units receive the same periodic input, and the phase of the latter is *not* reset after each firing [15].

III. THE POOLED SPIKE TRAIN

Our main results hinge upon the statistical description of the point process formed by the pooled discharge trains of a large number of units in parallel. To introduce the description of the summed spike train, let us recall that, similarly to the central limit theorem that states that the sum of a large number of independent identically distributed random variables becomes a Gaussian random variable, the sum of independent renewal point processes tends to a Poisson process [16]. In other words, inter-event intervals of the pooled point process are independent exponentially distributed random variables, and the intensity of the Poisson process is the sum of the rates of the individual processes. For example, the pooled spike train of a large number of LIFMs in parallel stimulated by independent white noise, without any other stimulation, forms a Poisson process, whose intensity λ is the sum of the discharge rates of the individual neurons. An equivalent statement is that the probability of having a discharge during an infinitesimal time interval of length dt is $\lambda\,dt$. This description puts the emphasis on the temporal homogeneity of the Poisson process since it indicates that the events occur with the same probability at any time.

When a non-constant stimulation, such as a periodic sine-like input current, is added to the units, the individual spike trains are no longer stationary. This character is also apparent in the pooled spike train: at times spikes are clustered and at others they are far apart. This observation indicates that the pooled spike train is not a homogeneous Poisson process (HPP) anymore since it displays temporal inhomogeneities. There is a time-dependent intensity function $\lambda(t)$ such that the probability that an event occurs between t and $t+dt$ is given by $\lambda(t)\,dt$. In other words, the process obtained by pooling the spike trains of a large number of units receiving a common input added to independent noise forms an inhomogeneous Poisson process (IPP). This process is characterized by a time dependent intensity function $\lambda(t)$ that represents the instantaneous firing rate of the ensemble of the units. Hence, $\lambda(t)$ suffices for the complete description of the pooled spike train. Therefore, when the output of the ensemble is modeled as an IPP, the main issue is to obtain an estimate of the rate λ. In the next paragraph, we show how in the case of a periodic stimulation, this can be achieved from the response of any given unit in the ensemble.

When the input signal is T-periodic, so is the intensity $\lambda(t)$, and the normalized cycle histogram h of the inhomogeneous Poisson process is given by

$$h(\theta) = \frac{T\lambda(T\theta/2\pi)}{2\pi\Lambda(T)} \quad \text{for} \quad 0 \leqslant \theta \leqslant 2\pi, \quad (3.1)$$

where $\Lambda(T) = \int_0^T \lambda(u)\,du$. The normalized cycle histogram gives the probability that a discharge occurs at a given phase. We remark that (1) the normalized cycle histogram of the pooled spike train is exactly the same as that of any individual unit in the ensemble, and, furthermore, (2) $\Lambda(T)$ represents the average number of discharges per input cycle and is given by $\Lambda(T) = NT/\langle t \rangle$ where $\langle t \rangle$ is the mean interspike interval of a single unit.

These two properties are of practical importance because they show that the discharge rate λ of the *ensemble* can be derived from the normalized cycle histogram and the mean interspike interval of a *single* unit.

In Appendix A, we describe how h and $\langle t \rangle$ can be obtained using a first-passage time approach. Our approach extends previous methods used for the analysis of the noisy LIFM with periodic modulation [3,17], in that it takes into account the phase distribution of the discharges.

For slow input signals, the intensity λ can also be estimated, under the quasi-static assumption, from the mean discharge rate of an individual unit in response to a constant stimulation [8]. Since the method presented in the previous paragraphs is valid independently from the modulation period, we have used it throughout our analysis, where emphasis was put on the processing of fast periodic signals.

The advantage of describing the pooled train as an IPP is that all relevant quantities can be derived from the estimate of the intensity $\lambda(t)$ and hence from h and $\langle t \rangle$ obtained from the response of a single unit. These will be described in a following paragraph. Before this, we discuss the validity of the statistical description of the pooled spike train.

In order to test the null-hypothesis according to which the ensemble spike train was a periodically modulated IPP, we first ''demodulated'' time, and then we tested whether the resulting point process was a HPP. These two steps are detailed in the following.

We estimated the time-dependent intensity λ of the process from the estimate of the normalized cycle histogram. The latter was obtained both by numerical simulations and by the numerical scheme presented in Appendix A. The time-step and discretization step for both the numerical integration of Eq. (2.1), and the algorithm in Appendix A were chosen so as to have agreement between the two methods, and such that decreasing the steps did not modify the results. Once the rate of the process was estimated, the point process of the discharge times was ''demodulated'' by a standard rescaling of time [16], according to

$$t \to t' = \Lambda(t) = \int_0^t \lambda(s)\,ds. \quad (3.2)$$

In other words, the rescaling of the time transformed the sequence of discharge times $u_1 < u_2 < \cdots < u_k < \cdots$ of the pooled spike train into the sequence $u_1' < u_2' < \cdots < u_k' < \cdots$, where each u_k' was obtained using Eq. (3.2). Practi-

cally, we performed this rescaling by replacing $\lambda(t)$ in Eq. (3.2) with the normalized rate $\nu(t)=T\lambda(t)/2\pi\Lambda(T)$. The use of ν avoided the estimation of the mean interspike interval $\langle t\rangle$.

If the original point process is an IPP, then the one obtained after demodulation is an HPP, and vice versa. Thus, testing the null-hypothesis according to which the original point process is an IPP of rate λ is equivalent to testing whether the demodulated process is an HPP. The latter can be done through several methods [18]. We used the following tests. First we estimated the mean inter-event interval of the process, and we tested whether the normalized inter-event interval histogram followed an exponential distribution. Then, we tested whether the successive intervals were independent. Precise description of the tests is given in Appendix B.

Other studies have used the periodically modulated IPP as an approximate model for the discharge train of a single unit [19,20]. This assumption has given satisfactory results when both the noise level and input amplitude are low. Therefore, in such cases, the ensemble spike train is the sum of independent IPPs, and satisfies the required conditions. However, in our work, we are interested in a wide range of noise levels and input amplitudes, where the response of a single unit in the ensemble cannot necessarily be described by such a process. This is due, for example, to the presence of the refractory period which forbids the occurrence of arbitrarily short intervals. Nevertheless, despite the fact that individual point processes are not IPP, when a large number of them are summed together, the resulting process is well described by a periodically modulated Poisson process. Figure 1 illustrates this point. The left and the right columns show the normalized interspike interval histograms of ensembles before and after demodulation, respectively, for $N=1$ (upper panel), $N=30$ (middle panel), and $N=300$. The solid lines in each panel show the distributions estimated from the normalized cycle histogram under the assumption that the process is a periodically modulated IPP. For a single unit, there is only a poor correspondence between the solid line and the histograms. This improves in $N=30$ where differences cannot be detected by a mere visual inspection and appear only in statistical tests. These discrepancies disappear for $N=300$, where even statistical tests do not detect significant differences.

As mentioned previously, one of the advantages of the description of the pooled spike train by a periodically modulated IPP is that all relevant quantities for the study of the input-output relation of the system can be obtained from the estimate of the rate λ, which is directly related to the characteristics of the response of a single unit through the normalized cycle histogram h, and the mean interspike interval $\langle t\rangle$. For example, the power norm C_0 and the normalized power norm C_1 are given by

$$C_0=\max_{\tau}\{\overline{A\sin(\Omega t)\lambda(t+\tau)}\}=A|a_1|=\frac{2AN|\alpha_1|}{\langle t\rangle}, \tag{3.3}$$

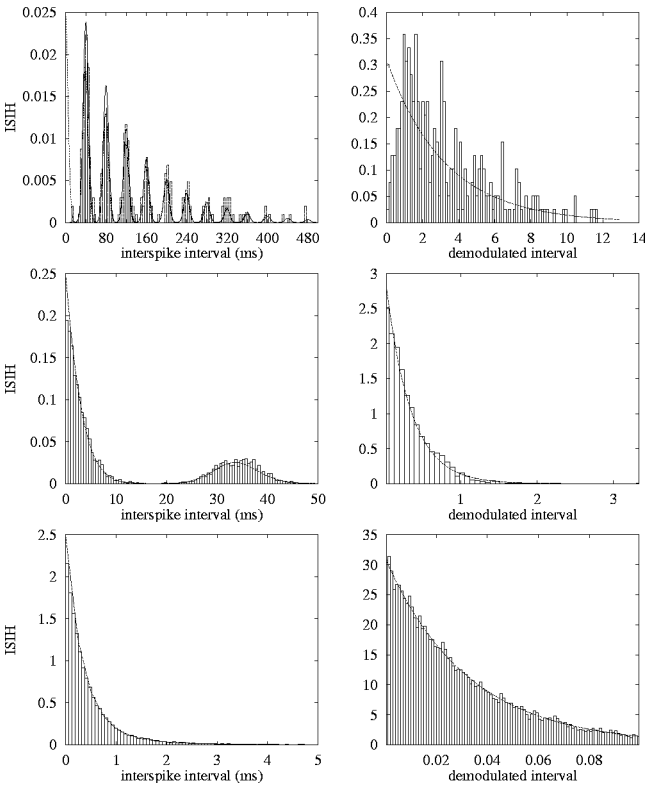

FIG. 1. Normalized interspike interval histograms before (left column) and after (right column) demodulation for $N=1$ (upper panels), $N=30$ (middle panels), and $N=300$ units (lower panels). Left column: abscissas: interspike interval duration in milliseconds; ordinates: probability density in kilohertz. Right column: abscissas: normalized interspike interval (dimensionless); ordinates: probability density (dimensionless). Model parameters: $\tau=5$ ms, $T=40$ ms, $V_r=10$ mV, $V_0=0$ mV, $S=15$ mV, and $D=0.5$ mV/(ms)$^{1/2}$.

$$C_1=\frac{C_0}{\sqrt{\overline{A^2\sin^2(\Omega t)}\,\overline{(\lambda(t)-\overline{\lambda(t)})^2}}}=\frac{|a_1|}{\sqrt{\sum_{q\geqslant 1}|a_q|^2}}$$

$$=\frac{|\alpha_1|}{\sqrt{\sum_{q\geqslant 1}|\alpha_q|^2}}, \tag{3.4}$$

where overbar is time average over one cycle, that is, $\overline{x(t)}=1/T\int_0^T x(t)dt$, and a_q and α_q are the coefficients of the Fourier expansion of $\lambda(t)$ and $h(\theta)$, respectively, given by

$$a_q=\frac{1}{T}\int_0^T\lambda(t)e^{-qj\Omega t}dt, \tag{3.5}$$

$$\alpha_q=\frac{1}{2\pi}\int_0^{2\pi}h(\theta)e^{-qj\theta}d\theta. \tag{3.6}$$

For the study of SR, an important measure is the signal-to-noise ratio (SNR), which for an IPP is defined as [19]

$$S = 10\log_{10}\left(\frac{2|a_1|^2}{a_0}\right) = 10\log_{10}\left(\frac{8N|\alpha_1|^2}{\langle t\rangle}\right).$$

The expressions of the above quantities clarify the influence of N for large ensembles: C_0 and S increase linearly with N and $\log N$, respectively, while C_1 is independent from the size of the ensemble. These dependencies are valid for large ensembles for which the discharge train can be described by an IPP. They indicate that the properties of the system are mainly determined by h and $\langle t\rangle$. For example, in order to investigate the influence of noise amplitude on these quantities, and see whether they are maximized at a particular noise level, we can as well consider the dependence on the noise amplitude of $c_0 = C_0/(AN)$ and $s = S - \log N$, which do not depend explicitly on the size N of the ensemble. Section IV A deals with the influence of noise on C_1 and the other measures of the input-output fidelity.

In the temporal coding scheme, the key assumption is that units in the ensemble fire reliably close to a given phase of the input signal. The shape of $\lambda(t)$ reflects such a preferential phase φ_p, in that this function presents marked peaks at $\varphi_p + kT$. The firing precision, denoted P, is then the ratio of the peak height, defined as the difference between the maximal and the minimal values of λ during one stimulus cycle, to the width w at half peak. This is similar to the precision used in [5]. Thus we have

$$P = \frac{\lambda_M - \lambda_m}{w}, \tag{3.7}$$

where $\lambda_M = \max\{\lambda(t):0 \leqslant t < T\}$, $\lambda_m = \min\{\lambda(t):0 \leqslant t < T\}$, and $w = t_2 - t_1$, with $\lambda(t_2) = \lambda(t_1) = (\lambda_M + \lambda_m)/2$ and $0 \leqslant t_1 < t_2 \leqslant T$. Using Eq. (3.1), and the fact that $\Lambda(T) = NT/\langle t\rangle$ we can define

$$p = \frac{T}{4\pi^2 N}P = \frac{1}{\langle t\rangle}\frac{h_M - h_m}{W}, \tag{3.8}$$

where $h_M = \max\{h(\theta):0 \leqslant \theta < 2\pi\}, h_m = \min\{h(\theta):0 \leqslant \theta < 2\pi\}$, and $W = 2\pi w/T$. The quantity p is proportional to the precision, yet it does not depend on the number of units in the ensemble, showing that the precision increases linearly with the number of units once the ensemble is large enough for the IPP assumption to hold. Besides the fact that p is independent from N, another advantage of using this quantity is that it can be computed directly from the normalized cycle histogram and the mean interspike interval of a single unit. In Sec. IV B we describe how this quantity varies with noise.

IV. INFLUENCE OF NOISE

In this section, we examine how changing the noise intensity modifies input-output fidelity and discharge timing precision in the response of the ensemble of LIFMs to a sinelike periodic signal. In this way, we link the optimal noise values which maximize the various criteria to the corresponding discharge patterns through the normalized cycle histogram h. At first, in Sec. IV A, we consider how the normalized power norm varies with the noise amplitude, for both sub and suprathreshold stimulations. We also mention how the other two measures, namely the power norm and the SNR, vary with noise. Next, in Sec. IV B, we examine the influence of noise on firing precision.

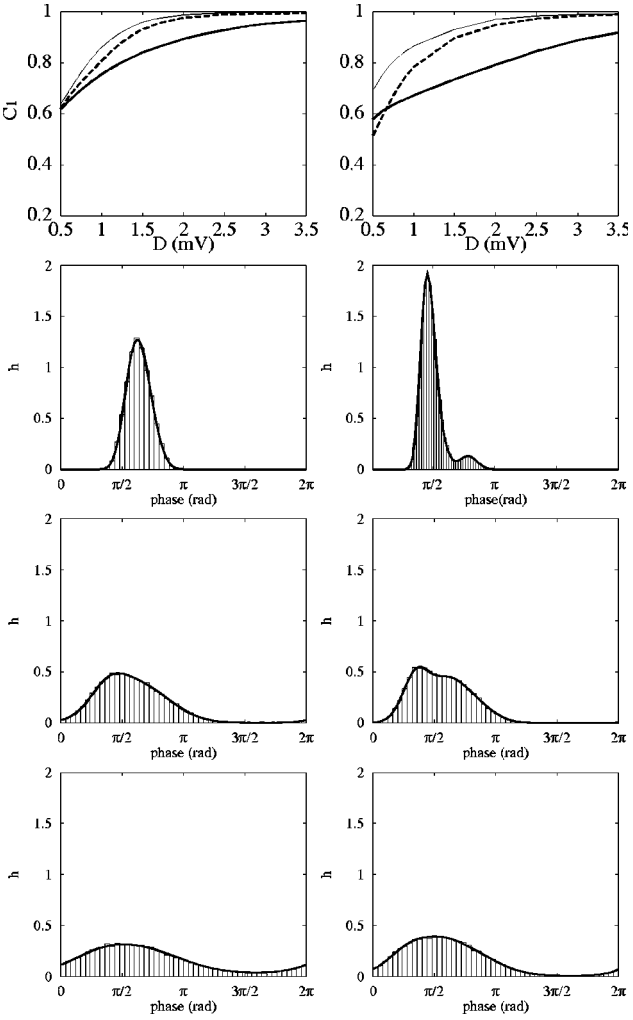

FIG. 2. Upper row: abscissae: noise intensity D in (millivolt) over (millisecond)$^{1/2}$; ordinates: normalized power norm C_1 (dimensionless) for period $T = 10$ ms (thick solid line), $T = 50$ ms (dashed line), and $T = 100$ ms (thin solid line). Second to fourth rows from top: abscissae: input phase at a discharge in radian; ordinates: normalized cycle histograms h (dimensionless) of a single neuron for a period $T = 50$ ms and three different noise intensities $D = 0.5$ mV/(ms)$^{1/2}$ (second row), $D = 1.5$ mV/(ms)$^{1/2}$ (third row), and $D = 2.5$ mV/(ms)$^{1/2}$ (fourth row). The histograms were computed using both numerical resolution of Eq. (2.1) (box graph) and the method described in Appendix A (solid line graph). Left column: subthreshold modulation amplitude $A' = A\tau/\sqrt{1+(\Omega\tau)^2} = 3.5$ mV. Right column: suprathreshold modulation amplitude $A' = 6$ mV. Model parameters $\tau = 5$ ms, $V_r = 10$ mV, $V_0 = 0$ mV, and $S = 15$ mV.

A. Input-output fidelity

The two upper panels in Fig. 2 show how C_1 changes with the noise amplitude D, for subthreshold (left panel) and suprathreshold (right panel) modulations with three different periods. All six curves increase with the noise level and saturate at one. This effect is similar to the no-tuning effect reported in the case of weak aperiodic input signals [7–9]. It can be explained in terms of the ''shape'' of the normalized

cycle histogram h. Indeed, C_1 measures the relative importance of $|\alpha_1|$, that is the first coefficient in the Fourier expansion of h. When C_1 tends to one, it indicates that the Fourier coefficients of order higher than one tend to zero, which in turn implies that h takes on progressively a sinelike shape. This is illustrated in the six lower panels in Fig. 2, which show h for a fixed period ($T=50$ ms), at three different noise levels, for the subthreshold (left column) and suprathreshold (right column) periodic modulations. At low noise levels, h displays a sharp peak (second row from top), which broadens as the noise amplitude is increased (third row from top), and eventually becomes sinelike (lower row) at higher noise levels. As the nonlinearities are reduced, the higher order coefficients of the Fourier expansion vanish. Thus, the no-tuning effect reflects the fact that as the noise amplitude increases, the ensemble firing rate becomes progressively like a sine wave. For suprathreshold periodic stimulation, these results are in agreement with the experimental data reported by French *et al.* [21] who evaluated the Fourier coefficients of the cycle histogram of a periodically modulated sensory neuron in the presence of noise, as well as other studies who reported that nonlinear distortions in cycle histograms decrease with the noise level (for a review see [1]).

The progressive linearization of the shape of h occurs jointly with the decrease of its amplitude given by $|\alpha_1|$. This is of importance for the determination of C_0 and the SNR. For a fixed number of neurons and a given input amplitude, C_0 is proportional to the ratio between $|\alpha_1|$ and $\langle t\rangle$, while SNR evolves in the same way as the ratio between $|\alpha_1|^2$ and $\langle t\rangle$. Both $|\alpha_1|$ and $\langle t\rangle$ tend to zero as the noise amplitude is increased. The former because the cycle histogram becomes flat, and the latter because shorter interspike intervals become more probable. The relative speed with which these two quantities decrease determines the behavior of the power norm C_0 and the SNR. For the parameter range considered, for both subthreshold (left column) and suprathreshold modulation (right column), c_0, and therefore C_0, increases and stabilizes at a plateau (upper row), while s (and hence the SNR) is hump shaped (second row from top), i.e., it is maximized at an intermediate noise level (Fig. 3). The hump is more pronounced for the subthreshold input. The corresponding values of $|\alpha_1|$ and $\langle t\rangle$ are shown in lower four panels of Fig. 3.

These results indicate that the no-tuning effect observed for the noise versus the normalized power norm, does not necessarily hold for other measures of the input-output fidelity which take into account the fact that the amplitude of the output rate decays down to zero as the noise is increased. Such measures, as for instance the SNR, may be maximized at intermediate noise amplitudes reflecting a compromise between the increase in C_1 and the decrease in $|\alpha_1|$ (left panel of the second row from top in Fig. 3).

To our knowledge, no general results on the speed at which the two quantities $|\alpha_1|$ and $\langle t\rangle$ tend to zero with increasing noise levels is available. Our numerical investigations (not shown) indicate that the variations of C_0 and the SNR with the noise amplitude can depend on other model parameters. As the main concern of the present section was to determine the range of noise where the no-tuning effect for C_1 takes place, we will not detail this point any further. This issue together with a detailed description of the dependence of the shape of C_1 and C_0 on model parameters will be addressed elsewhere.

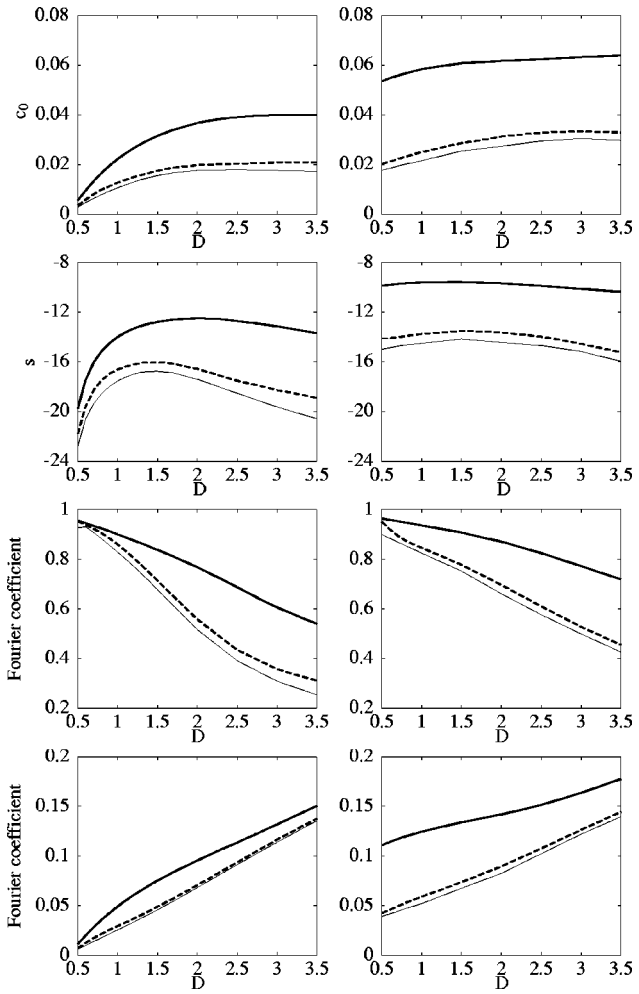

FIG. 3. Upper row: abscissas: noise intensity D in mV/(ms)$^{1/2}$; ordinates: power norm $c_0=C_0/(AN)=|\alpha_1|\times 2/\langle t\rangle$ in kilohertz. Second row from top: abscissas: noise intensity D in millivolt; ordinates: $s=S-\log N$ (decibel), where S is the SNR. Third row from top: abscissas: noise intensity D in mV/(ms)$^{1/2}$; ordinates: Fourier coefficient $a_0/N=2/\langle t\rangle$ in kilohertz for h. Lower row: abscissas: noise intensity D in mV/(ms)$^{1/2}$; ordinates: Fourier coefficient α_1 (dimensionless) for λ. Left panels: subthreshold stimulations $A'=A\tau/\sqrt{1+(\Omega\tau)^2}=3.5$ mV. Right panels: suprathreshold stimulations $A'=6$ mV. For all the panels, modulation period is $T=10$ ms (thick solid line), $T=50$ ms (thick dashed line), and $T=100$ ms (thin solid line). Model parameters: $\tau=5$ ms, $V_r=10$ mV, $V_0=0$ mV, and $S=15$ mV.

B. Firing precision

In the previous section, we were mainly concerned with the relation between the discharge rate of the ensemble with the input signal. The measures of transmission fidelity that were used were related to this aspect. Consequently, the noise-induced enhancement in signal transmission occurs for noise levels such that the normalized cycle histogram re-

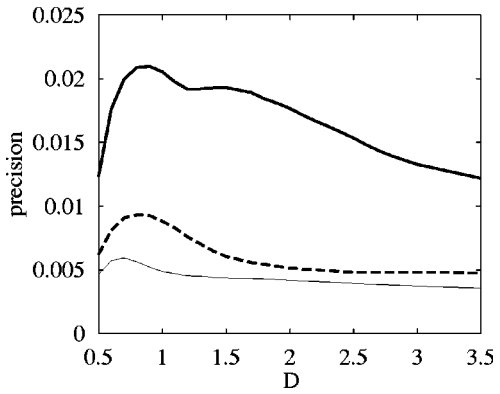

FIG. 4. The evolution of p [Eq. (3.8)] for different modulation period, $T=10$ ms (thick solid line), $T=50$ ms (thick dashed line) and $T=100$ ms (thin solid line). Abscissa: noise intensity D in mV/(ms)$^{1/2}$; ordinate: $p=(T/4\pi^2N)P$ in kilohertz per radian, where P is the spike timing precision. Model parameters: $\tau=5$ ms, $V_r=10$ mV, $V_0=0$ mV, $S=15$ mV, and $A'=3.5$ mV (subthreshold modulation).

sembles the input waveform. In this section, we consider the influence of noise on the discharge time precision defined by Eq. (3.7).

Figure 4 shows the evolution of p (Eq.(3.8)) for subthreshold periodic modulations with periods $T=10$ ms (thick solid line), $T=50$ ms (thick dashed line) and $T=100$ ms (thin solid line). The amplitudes of the input signals were adjusted so as to have the same membrane potential oscillation amplitudes. These values are the same as in upper left panel in Fig. 2 and upper two panels of left column in Fig. 3 where the various measures of the input output fidelity were represented. For all three subthreshold periodic signals, the precision increases at low noise levels, goes through a maximum, and then decays progressively as the noise amplitude increases.

The behavior of the precision as function of the noise level can be understood in terms of the relative contributions of the two terms that compose it, namely $1/\langle t\rangle$ and $(h_M-h_m)/W$. The former is the inverse of the mean interspike interval duration. For subthreshold modulation, this quantity is zero in the deterministic limit when $D=0$. As the noise level is increased, $1/\langle t\rangle$ grows and tends to infinity at the limit of large noise intensities. The second term has the converse behavior i.e., it decays progressively from infinity to zero as the noise level is increased. Indeed, it measures the sharpness of the peak of h. At low noise levels, this quantity tends to infinity, as the neurons mainly fire when the membrane potential oscillations reach their maximal value. This strong affinity to discharge at a preferential phase is reflected as a marked narrow peak in the normalized cycle histogram (e.g., second panel from top in left column of Fig. 2). As the noise intensity is increased, the height of the peak decreases and its base widens (left panels in two lower rows of Fig. 2). This leads to a progressive decrease in $(h_M-h_m)/W$. Finally, in the limit of large noise, h flattens, i.e., $h_M\simeq h_m$, while W tends to 2π. As a result, $(h_M-h_m)/W$ tends to zero. Thus the unimodal shape of the precision is the result of the interplay between two factors with opposite tendencies as the noise level is increased.

For suprathreshold stimulation, the situation is different. The precision decays monotonously as the noise level is increased (data not shown). Indeed, whereas $(h_M-h_m)/W$ has the same noise dependency as in the case of subthreshold stimulation, that is, decreasing from infinity to zero as the noise is increased, the quantity $1/\langle t\rangle$ tends to a finite nonzero value as D tends to zero.

Thus, as in the case for a single stimulation [5], noise of appropriate amplitude can enhance the precision for subthreshold periodic stimulation, however, it only deteriorates the precision for suprathreshold input signals. In the next section, we compare the discharge characteristics of single units and ensembles in regimes of high precision with those in regimes of high-fidelity, in order to better shed light on the similarities and differences between them.

C. Comparison between high-fidelity and high precision regimes

On the one hand, Sec. IV A confirmed that, in agreement with previous studies [7–9], noise of appropriate amplitude can enhance the input-output fidelity in an ensemble of LIFMs receiving subthreshold periodic stimulation. On the other hand, Sec. IV B extended the work in [5] by showing that tuning noise can enhance discharge precision in response to subthreshold period stimulation. The purpose of the present section is to compare the regimes that lead to optimal behavior in each situation.

Comparison of Fig. 4 with upper left panel in Fig. 2 and upper two panels of left column in Fig. 3 reveals that the noise intensities that maximize the firing precision are lower than those that saturate C_1 and C_0 or maximize the SNR. This is consistent with our interpretation of the relationship between the noise-induced changes and the shape of the normalized cycle histogram h, and their implication for the various criteria used to assess input-output fidelity and discharge timing precision. Indeed, the former reach their optimal values when the cycle histogram takes on a sinelike shape, whereas the latter is maximal when h has a marked peak.

In order to clarify the implications of this difference in the shape of h on the discharge characteristics of the units within the ensemble, we have represented (from top to bottom in upper panels of Fig. 5) the input current, the spike train emitted by four neurons, the pooled trains of one thousand units, and the discharge rate of the same ensemble for three different noise levels [$D=0.9$ (left column), $D=2$ (middle column) and $D=3.5$ (right column)]. The two lower panels in each column represent the corresponding normalized cycle histogram and the ISIH of a single neuron. The first two noise intensities represent the optimal values for the precision ($D=0.9$) and the SNR ($D=2.0$). At the third one ($D=3.5$), C_1 is larger than 0.95. Visual inspection of the spike trains of the individual units reveals that for none of the noise levels, do the units discharge at all input cycle. This is due to the fact that the input period $T=10$ ms is relatively short. Besides this similarity, the main difference that stands out is that, as expected, the number of discharge within the observation window increases with the noise level. However, mere visual inspection of these spike trains does not clarify the origin of the differences between them. The difference between the three noise levels are more striking at the level

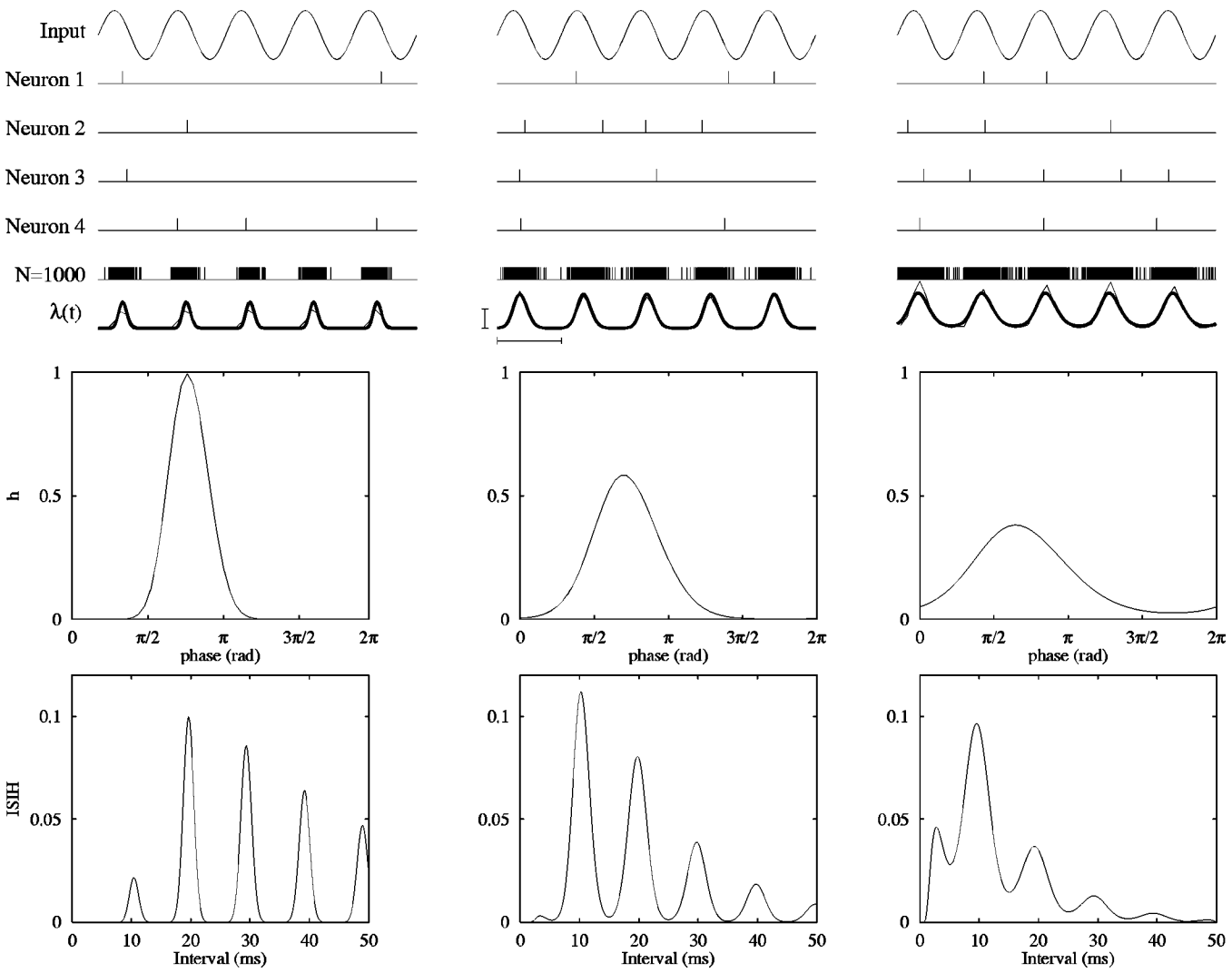

FIG. 5. Upper row: we depict input current, the spike train emitted by four neurons, the pooled spike train for $N=1000$, and instantaneous discharge rate $\lambda(t)$. From the pooled spike train, we calculate histogram and adjust the height to satisfy the area at one cycle is equal one. Then we superimpose it to $\lambda(t)$. Abscissas in upper row: time in millisecond; ordinates in upper row: unitless except for the last graph $\lambda(t)$ in kilohertz. Horizontal mark in upper middle panel corresponds to the length of modulation period $T=10$ ms. Vertical mark in upper middle panel corresponds to the size of $\lambda=0.1$ in kilohertz. Middle row: abscissas: input phase at a discharge in radian; ordinates: normalized cycle histogram h (dimensionless) of a single neuron. Lower row: abscissas: interspike interval in millisecond; ordinates: interspike interval histogram of a single neuron in kilohertz. Left column: noise intensity is $D=0.9$ mV/(ms)$^{1/2}$, which gives the hump of the precision (Fig. 4). Middle column: noise intensity is $D=2.0$ mV/(ms)$^{1/2}$, which gives the hump of SNR (left panel in the middle row of Fig. 3). Right column: noise intensity is $D=3.5$ mV/(ms)$^{1/2}$, at which C_1 is larger than 0.9 (upper left panel in Fig. 2). Model parameters: $T=10$ ms, $\tau=5$ ms, $V_r=10$ mV, $V_0=0$ mV, $S=15$ mV, and $A'=3.5$ mV (subthreshold modulation).

of the pooled trains. At $D=0.9$, this train is clearly formed by a periodic succession of bursts occurring around a preferential input phase. At $D=2$, bursts are still visible, however the distinction between successive bursts is less marked than for $D=0.9$. Finally, for $D=3.5$, the pooled train is densely packed, and the input periodicity is less visible. The discharge rates of the ensembles for the three noise levels are represented under the corresponding spike trains. That of the lowest noise level is a succession of sharp peaks separated by the modulation period. For the intermediate noise level, the peaks are still present, albeit they are wider, and finally at the highest noise level, the rate resembles a sine function. This progressive change in the shape of the firing is also present at the level of the normalized cycle histograms of individual units. To clarify the origin of the difference between these regimes, we provide a heuristic description of the discharge characteristics of the neurons that would maximize the precision, the SNR or C_1.

If all discharges occur exactly at the same input phase in all input cycles, then the spike timing precision is maximal. This ideal situation is possible when individual units phase lock to a suprathreshold periodic input, in the absence of noise. When the input signal is subthreshold, however, some noise is necessary to elicit discharges. At low noise levels, discharges are possible only when the membrane potential reaches its maximal value within each cycle. Thus, spikes occur narrowly spread around a given phase, the lower the noise level and the smaller the width of this distribution. However, in this regime, especially when the input modulation is fast compared to the membrane charge-discharge time constant, single units do not fire at every input cycle, but rather, unreliably once every several cycles, with a large

variation in the number of cycles separating two successive discharges. Tateno et al. [22] have coined the term stochastic phase locking to describe this form of firing pattern (see also [23]): spikes display a strong preferential phase leading to a cycle histogram with a marked peak, while, in contrast with deterministic phase-locking the spike train is not periodic. In other words, in stochastic phase locking, a neuron fires on average r spikes per cycle, with the discharges occurring near the preferential phase. At low noise levels, and for fast signals, r is smaller than one. This can be seen in the discharge trains of the four neuron models in the upper left panels of Fig. 5. The ISIH of any of these units resembles the one represented in the bottom left panel of the same figure. The ISIH has peaks at multiples of the modulation period, a signature of skipping. Interestingly the peak height at the modulation period itself is the lowest among those visible. In other words, at this noise level, the individual units do not transmit reliably the input period. The effect of pooling the response of a large number of units is that a proportion r of them will fire at every input cycle. Due to the central limit theorem, there will be little variability in the proportion of units firing at each cycle, when the ensemble is large enough. At low noise level, the proportion r is small, so that despite the fact that the normalized cycle histogram has a sharp peak, the discharge timing precision is low: there are not enough units responding at each cycle. Increasing the noise level improves the response amplitude r, at the same time as it widens the normalized cycle histogram. The optimal noise level that maximizes the precision represents a balance between these two effects.

The situation for the SNR is different in that this quantity is not sensitive directly to the peak height of the normalized cycle histogram as the precision, but rather to the first coefficient of its Fourier expansion [Eq. (3.6)]. In this way, the change of the SNR with the noise level is more subtle than that of the precision. Nevertheless, at low noise levels, the SNR is small because in this regime the mean ISI $\langle t \rangle$ is very large, and $1/\langle t \rangle$ dominates the evolution of the SNR. When the noise level is large enough, however, $|\alpha_1|^2$ becomes preponderant. The value of $|\alpha_1|^2$ depends on two factors, one the dynamical range of the response, that is the amplitude of h (i.e., $h_M - h_m$), the other is the similarity between the shape of h and a sine function. However, in contrast with the precision, the SNR does not depend on the width of h. This is the main reason why the SNR is maximal at a larger noise intensity than the precision. Nevertheless, at this noise level, the individual units still display skipping, i.e., the ISIH has marked peaks at the multiples of the modulation period. Interestingly, the peak height at the modulation period is the largest, and significantly larger than for $D=0.9$. There is also a small hump appearing at ISIs shorter than the modulation period, due to the spread in h.

Finally, the situation represented in the right panels where C_1 takes a large value is different from the two previous cases in that, as already explained in Sec. IV A, this quantity is independent from the dynamical range, and measures the relative importance of $|\alpha_1|$ in comparison with the other coefficients. Therefore, C_1 tends to one, so h becomes flat. Despite the fact that h strongly resembles a sine function at this noise level, the discharges of the individual units still display some skipping, as attested by the sparse discharge trains of the four units (upper right panels Fig. 5) and the peaks at multiples of the modulation period in the ISIH. However, in contrast with the two previous cases, a given unit can now discharge several times during a single input cycle.

In summary, the three measures of the input-output transformation in the ensemble reach their optimal level for noise levels that correspond to different discharge characteristics at the level of individual units. Furthermore, our results illustrate the beneficial effect of pooling the response of units with the ensemble to improve both input-output fidelity and spike timing precision in the case of fast periodic signals, that can be below the resolution limit of the individual units.

V. DISCUSSION

We studied the response of an ensemble of LIFMs to a sinelike periodic signal in the presence of noise. The main conclusions of our study can be summarized as follows.

(i) The spike train generated by large ensembles of LIFMs receiving a common periodic sine-like input and independent noise can be accurately modeled by a periodically modulated IPP. This approach is advantageous for the description of the response of the system, in that all relevant quantities can be computed from the intensity of the IPP. Previous studies have used a similar assumption for the description of the discharge times of single units. As argued in [20], in the case of single units, this hypothesis approximately holds for low noise levels, but breaks down for other parameter values. For ensembles, however, the range of validity of the statistical model is wider than that for single units, and this allowed us to describe the response of the system to both sub and suprathreshold stimulations, for a wide range of noise amplitudes.

In [24], the event times of a periodically modulated system in the presence of noise have also been modeled by an IPP. However, in [24], the assumption is that the response of the system is determined *a priori* by an IPP so that the function giving the instantaneous rate is an exponential and does not change with the noise level, whereas in our analysis, once the output of the system is known, we show, *a posteriori*, that it can be statistically modeled by an IPP, so that it is the very shape of the rate function that depends on the noise.

(ii) The intensity of the IPP can be estimated from the response of a single unit in the ensemble, and we developed a method for the description of the response of a single LIFM in response to periodic modulation with noise. This method follows [22], and relies on the iterations of a stochastic phase transition operator, which generalizes the concept of phase transition curve used to describe the response of oscillators to periodic stimulation, to the case of stochastic systems. In this way, the normalized cycle histogram of the system is the invariant density of this operator [25,26]. In a companion publication, we will present a study of the influence of noise on this operator.

(iii) There is a direct link between the normalized cycle histogram h and the mean ISI $\langle t \rangle$ of any single unit within the ensemble and measures of the input-output fidelity such as C_0, C_1 and the SNR, as well as spike timing precision. This relation clarifies the discharge characteristics that maxi-

mize each of these quantities. (a) The ''no-tuning effect,'' that is, the steady increase of C_1 and progressive saturation at a maximal level as the noise intensity is increased [7] results from the reduction of nonlinear distortions in h. This phenomenon had been first observed in [21] for suprathreshold modulation (see also [1] for a review and [8,9] for more recent discussions). (b) Other measures of input-output fidelity such as SNR do not necessarily display the no-tuning phenomenon. Instead, they are maximized at intermediate noise levels that represent a compromise between the linearization of h and the dynamical range in the response. (c) Discharge-timing precision to subthreshold modulation can be enhanced by noise. This extends the results in [5], where this phenomenon was first reported in the response of an ensemble to a single post-synaptic potential. The possible biological implication of this phenomenon is that even highly specialized neuronal assemblies known to detect minute differences below the temporal resolution of individual units that compose them, can actually benefit from the presence of some noise. In other words, noise does not necessarily disrupt temporal coding, rather, if tuned properly, it can improve the reliability of ensembles. Whether such a tuning is actually present in nervous systems remains to be elucidated. (d) Comparison of discharge characteristics at noise levels that maximized input-output fidelity and spike-timing precision clearly showed that these correspond to distinct regimes. In the former, discharges occur at all input phases, whereas in the latter, spikes display a strong preferential phase. In both cases pooling the spike trains of the units within the ensemble balances the variability in the response of individual units.

In summary, our results show that not only rate coding, but also temporal coding can be improved by the presence of noise. However, the noise levels that maximize input-output fidelity are significantly different from those that enhance spike timing precision. Our study was concerned with *possible* beneficial effects of noise in signal processing and transmission in nervous systems. At this point, experimental measurements of the variability of individual units discharges would be necessary to determine whether the noise in neuronal ensembles is indeed close to optimal levels that maximize either the spike-timing precision or the input-output fidelity.

ACKNOWLEDGMENTS

A.R. would like to express her thanks to Pr. Sato and the members of his laboratory for their hospitality during her visit which was partially supported by Monbusho. A.R. and K.P. would like to thank Dr. J. Pham for his help regarding the algorithms for testing Poisson processes.

APPENDIX A: THE RESPONSE OF A SINGLE UNIT

When the periodic signal is exogenous, the membrane potential and the threshold are reset after the discharge but not the phase of the external input [15]. Hence, the phase of the signal at the firing is a random variable with probability density function h. For the calculation of h for a single noisy LIFM, we follow the approach introduced in [22,25,26]. This method relies on the numerical evaluation of the interspike interval distribution from the first passage times of an Ornstein-Uhlenbeck process through a time-dependent boundary rather than the numerical resolution of Eq. (2.1). Let the nth interspike interval, i.e., the time interval between $(n-1)$th and nth firing of an LIFM described by Eq. (2.1), be t_n, and let the nth phase, i.e., the phase of input sinusoidal current at nth firing, be θ_n. Then the first firing occurs at $t=t_1$ and it follows $\theta_1=\Omega t_1+\theta_0(\mathrm{mod}\,2\pi)$. Similarly, the second firing occurs at $t=t_1+t_2$ and $\theta_2=\Omega(t_1+t_2)+\theta_0(\mathrm{mod}\,2\pi)$. We are interested in the sequences t_n and θ_n. Since both of these are random variables, we compute their respective probability density function (pdf) denoted by $i_n(t)$ and $h_n(\theta)$. Assuming that $V(0)=V_0$, we have $i_1(t)=g(t|\theta_0)$ and $h_1(\theta)=f(\theta|\theta_0)$. $g(t|\theta)d\theta$ is the probability that a discharge occurs in $(t,t+dt)$. $f(\phi|\theta)d\phi$ is the conditional probability that the firing phase is in $(\phi,\phi+d\phi)$ given the previous firing phase θ, and f is described as

$$f(\phi|\theta)=\frac{1}{\Omega}\sum_{k=0}^{\infty} g\left(kT+\frac{\phi-\theta}{\Omega}\middle|\theta\right).$$

Similarly, for $n=2$, $i_2(t)=\int_0^{2\pi} g(t|\theta)h_1(\theta)d\theta$ and $h_2(\phi)=\int_0^{2\pi} f(\phi|\theta)h_1(\theta)d\theta$. In general,

$$i_n(t)=\int_0^{2\pi} g(t|\theta)h_{n-1}(\theta)d\theta, \quad n=1,2,\ldots,$$

$$h_n(\phi)=\int_0^{2\pi} f(\phi|\theta)h_{n-1}(\theta)d\theta, \quad n=1,2,\ldots.$$

When $n\to\infty$, i_n and h_n converge to invariant distributions i_∞ and h_∞. Let us define the stochastic phase transition operator $\mathcal{P}$ as $h_n(\phi)\equiv\mathcal{P}h_{n-1}(\phi)$. It is a Markov operator with kernel $f(\phi|\theta)$. Applying the Markov operator iteratively to the pdf h_0 of the initial phase, we can obtain h_n as $h_n=\mathcal{P}h_{n-1}=\cdots=\mathcal{P}^n h_0$. As n goes to infinity, we get invariant distribution h_∞ i.e., h uniquely, and this function corresponds to the eigenfunction of $\mathcal{P}$ belonging to the eigenvalue 1.

The scheme described above provides a method for the numerical computation of h_∞. Indeed, $g(t|\theta)$ corresponds to the first passage time pdf of an Ornstein-Uhlenbeck process through an appropriate time varying boundary and can be numerically evaluated using the algorithm in [27]. Then $g(t|\theta)$ can be used to compute iteratively h_n and i_n until reaching the invariant densities. Finally, let us remark that h_∞ is the normalized cycle histogram h, so that λ can be derived from h_∞ using Eq. (3.1) together with the fact that $\Lambda(T)=TN/\langle t\rangle$ where $\langle t\rangle=\int_0^\infty t i_\infty(t)dt$ is the mean interspike interval.

In Fig. 3, we have compared h obtained using our method (solid line) explained in this appendix with numerical simulation (Euler scheme) of corresponded stochastic differential equation Eq. (2.1) (histogram). The histogram of h is made by 30 000 data of the firing time. We have tested whether the null hypothesis, which, in these two histograms is the same, is rejected or not. For all parameter sets in Fig. 3, chi-square test did not reject the null hypothesis, that is to say, the solid line of h obtained by our method fit the histogram by the numerical simulation.

APPENDIX B: STATISTICAL TESTS

Let random variables X_t, $t=1,\cdots,n$ denote a series of events, i.e., $X_t=1$ if an event occurs at time t, and 0 otherwise. We denote by I_t the time interval between events X_t and X_{t+1}.

$\{X_t\}$ form a Poisson Process with intensity λ if I_t is independently exponentially distributed with parameter λ. Thus when given a series of events, to test whether the corresponding point process is Poisson, we need to test whether (i) intervals are independent, and (ii) they are exponentially distributed.

The statistical test of the independence of I_t that we used is based on serial correlation coefficient. An estimation of these coefficients from a sample, when $E(I)$ is not known, is

$$\hat{\rho}_k=\frac{\sum_{t=1}^{n-k}(I_t-\tilde{I}'_k)(I_{t+k}-\tilde{I}''_k)}{\sqrt{\sum_{t=1}^{n-k}(I_t-\tilde{I}'_k)^2\sum_{t=1}^{n-k}(I_{t+k}-\tilde{I}''_k)^2}},$$

where

$$\tilde{I}'_k=\frac{1}{n-k}\sum_{t=1}^{n-k}I_t,\quad \tilde{I}''_k=\frac{1}{n-k}\sum_{t=1}^{n-k}I_{t+k}.$$

$\hat{\rho}_k\sqrt{n-1}$ is asymptotically normally distributed so independence, i.e., null-hypothesis $H_0:\rho_1=0$, is rejected at level α if $|\widehat{\rho_1}|>c_\alpha/\sqrt{n-1}$ where c_α is read in a standardized normal table. To insure that there is no correlation of higher order, we also test whether ρ_k is significantly different from 0 for $k=1,\ldots,5$.

The statistical test of the exponential distribution, i.e., with null-hypothesis $H_0:F(x)=F_0(X)$, where $F(x)=1-e^{-\hat{\lambda}x}$, with $\hat{\lambda}=\Sigma i/n$ and $F_0(X)$ is the sample repartition of I_t, that we used is based on Cramer Von Mises Statistic:

$$n\omega^2=\frac{1}{12}+\sum_{t=1}^{n}\left[\frac{2t-1}{2n}-F(i_t)\right]^2,$$

where $i_1<i_2<\cdots<i_n$. The null-hypothesis H_0 is rejected with level $\alpha=0{,}05$ if $(1+0.16/n)n\omega^2>0.224$ (empirical results obtained by simulation. See Biometrika tables [28]).

[1] J.P. Segundo *et al.*, in *Origins: Brain and Self Organization*, edited by K. Pribram (Lawrence Erlbaum Associates, Hillsdale, NJ, 1994); K. Douglass, *et al.*, Nature (London) **365**, 337 (1993); J.E. Levin and J.P. Miller, *ibid.* **380**, 165 (1996); J.J. Collins, T.T. Imhoff, and P. Grigg, J. Neurophysiol. **76**, 642 (1996).

[2] H. Spekreijse, and H. Oosting, Kybernetik **7**, 22 (1970); A. Longtin, A. Bulsara, and F. Moss, Phys. Rev. Lett. **67**, 656 (1991); D.R. Chialvo and A.V. Apkarian, J. Stat. Phys. **70**, 375 (1993); A. Longtin, *ibid.* **70**, 309 (1993); X. Pei, K. Bachman, and F. Moss, Phys. Lett. A **206**, 61 (1995); J.J. Collins, C.C. Chow, and T.T. Imhoff, Phys. Rev. E **52**, 3321 (1995); J.J. Collins *et al.*, *ibid.* **54**, 5575 (1996); M. Stemmler, Network **7**, 687 (1996).

[3] A.R. Bulsara *et al.*, Phys. Rev. E **53**, 3958 (1996).

[4] A.R. Bulsara and L. Gammaitoni, Phys. Today **49(3)**, 39 (1996); L. Gammaitoni *et al.*, Rev. Mod. Phys. **70**, 223 (1998); F. Moss, D. Pierson, and D. O'Gorman, Int. J. Bifurcation Chaos Appl. Sci. Eng. **4**, 1383 (1994).

[5] X. Pei, L. Wilkens, and F. Moss, Phys. Rev. Lett. **77**, 4679 (1996).

[6] B.W. Knight, J. Gen. Physiol. **59**, 734 (1972).

[7] J.J. Collins, C.C. Carson, and T.T. Imhoff, Nature (London) **376**, 236 (1995).

[8] D.R. Chialvo, A. Longtin, and J. Müller-Gerking, Phys. Rev. E **55**, 1798 (1997).

[9] A. Neiman, L. Schimansky-Geier, and F. Moss, Phys. Rev. E **56**, 9 (1997).

[10] G. Rose and W. Heiligenberg, Nature (London) **318**, 178 (1985).

[11] H. Agmon-Snir, C.E. Carr, and J. Rinzel, Nature (London) **393**, 268 (1998).

[12] H.A. Braun *et al.*, Nature (London) **367**, 270 (1994).

[13] J.J. Hopfield, Nature (London) **376**, 33 (1995).

[14] W. Gerstner *et al.*, Nature (London) **383**, 76 (1996).

[15] P. Lánský, Phys. Rev. E **55**, 2040 (1997).

[16] D.R. Cox, *Renewal Theory* (Methuen & Co. Ltd., London, 1962).

[17] H.E. Plesser and S. Tanaka, Phys. Lett. A **225**, 228 (1997).

[18] D.R. Cox and P.A.W. Lewis, *Statistical Analysis of Series of Events* (Maehuen & Co. Ltd., London, 1966).

[19] K. Wiesenfeld *et al.*, Phys. Rev. Lett. **72**, 2125 (1994).

[20] D. Petracchi *et al.*, Int. J. Bifurcation Chaos Appl. Sci. Eng. **5**, 98 (1995).

[21] A.S. French, A.V. Holden, and R.B. Stein, Kybernetik **11**, 15 (1972).

[22] T. Tateno, S. Doi, S. Sato, and L.M. Ricciardi, J. Stat. Phys. **78**, 917 (1995); S. Doi, J. Inoue, and S. Kumagai, *ibid.* **90**, 1107 (1998); T. Tateno, *ibid.* **92**, 675 (1998).

[23] A. Longtin, Chaos **5**, 209 (1995).

[24] S.M. Bezrukov and I. Vodyanoy, Nature (London) **385**, 319 (1997).

[25] T. Shimokawa, K. Pakdaman, and S. Sato, Phys. Rev. E (to be published).

[26] T. Shimokawa *et al.*, Technical Report of IEICE, MBE **97-14**, 99 (1997) (in Japanese).

[27] V. Giorno, A.G. Nobile, L.M. Ricciardi, and S. Sato, Adv. Appl. Probab. **21**, 20 (1989). This method can be applied for constant drift term, so we transformed constant threshold into modulated threshold.

[28] E.S. Pearson and H.O. Hartley, *Biometrika Tables for Statisticians* (Cambridge University Press, Cambridge, England, 1996).